


ARTICLE



Targeting the DIO3 enzyme using first-in-class inhibitors effectively suppresses tumor growth: a new paradigm in ovarian cancer treatment

Dotan Moskovich^{1,2}, Yael Finkelshtein^{1,2}, Adi Alfandari^{1,2}, Amit Rosemarin^{1,2}, Tzuri Lifschytz³, Avivit Weisz⁴, Santanu Mondal⁵, Harinarayana Ungati⁵, Aviva Katzav⁴, Debora Kidron^{4,6}, Govindasamy Mugesh⁵, Martin Ellis^{1,6}, Bernard Lerer³ and Osnat Ashur-Fabian^{1,2} 

© The Author(s), under exclusive licence to Springer Nature Limited 2021, corrected publication 2023

The enzyme iodothyronine deiodinase type 3 (DIO3) contributes to cancer proliferation by inactivating the tumor-suppressive actions of thyroid hormone (T3). We recently established DIO3 involvement in the progression of high-grade serous ovarian cancer (HGSOC). Here we provide a link between high DIO3 expression and lower survival in patients, similar to common disease markers such as Ki67, PAX8, CA-125, and CCNE1. These observations suggest that DIO3 is a logical target for inhibition. Using a DIO3 mimic, we developed original DIO3 inhibitors that contain a core of dibromomaleic anhydride (DBRMD) as scaffold. Two compounds, PBENZ-DBRMD and ITYR-DBRMD, demonstrated attenuated cell counts, induction in apoptosis, and a reduction in cell proliferation in DIO3-positive HGSOC cells (*ES-2* and *KURAMOCHI*), but not in DIO3-negative normal ovary cells (*CHOK1*) and *ES-2* depleted for DIO3 or its substrate, T3. Potent tumor inhibition with a high safety profile was further established in HGSOC xenograft model, with no effect in DIO3-depleted tumors. The antitumor effects are mediated by downregulation in an array of pro-cancerous proteins, the majority of which known to be repressed by T3. To conclude, using small molecules that specifically target the DIO3 enzyme we present a new treatment paradigm for ovarian cancer and potentially other DIO3-dependent malignancies.

Oncogene (2021) 40:6248–6257; <https://doi.org/10.1038/s41388-021-02020-z>

INTRODUCTION

Iodothyronine deiodinase type 3 (DIO3) enzyme is the major inactivator of the biologically active thyroid hormone, 3,5,3'-triiodo-L-thyronine (T3). DIO3 catalytic core contains a unique amino acid, selenocysteine, which removes iodine atoms from the inner ring of its main substrate, T3, and produces 3,3'-diiodothyronine (T2), an inactive derivative [1]. The other deiodinase family members, DIO1 and DIO2, mainly activate T3 by releasing iodine from the outer ring of the pro-hormone T4 [2]. T3 mainly regulates differentiation and mitochondrial respiration and is therefore considered a tumor suppressor [3]. In several cancer types, DIO3 was shown to contribute to tumor proliferation by catabolizing T3, thus eliminating its anti-cancer activities [4–9]. We recently established the expression of DIO3 in high-grade serous ovarian cancer (HGSOC) and its involvement in disease progression [10]. This gynecological malignancy is responsible for the highest mortality from cancers of the female reproductive system [11, 12] and development of better treatment approaches is desired.

The role played by DIO3 in maintaining ovarian cancer proliferation suggests this enzyme as a logical target for inhibition. However, no specific DIO3 inhibitors were developed thus far [13], mainly due to the fact that this enzyme is an

integral homodimeric transmembrane protein that loses its activity upon purification [14]. Mugesh et al. developed synthetic compounds that contain selenyl groups and functionally mimic the DIO3 enzymatic activity with respect to deiodination and inactivation of T3 [15–19]. These biomimetics were utilized by our collaborative research group for the design of compounds that specifically inhibit the DIO3 enzyme. In this current work, we established, *in vitro* and *in vivo*, the efficacy of two best hit DIO3 inhibitors in HGSOC. This novel therapeutic paradigm may be applicable not only for ovarian cancer, but potentially to other DIO3-dependent cancer types.

RESULTS

High DIO3 expression is associated with lower survival in a subset of HGSOC patients

Our group has demonstrated by preclinical models a high expression of the DIO3 enzyme in HGSOC, with significant pro-mitogenic roles [10]. In order to explore DIO3 prognostic value in the clinical settings, we studied whether high DIO3 expression correlates with patients' survival. The gene expression was extracted from The Cancer Genome Atlas (TCGA) database

¹Translational Oncology Laboratory, Hematology Institute and Blood Bank, Meir Medical Center, Kfar-Saba, Israel. ²Department of Human Molecular Genetics and Biochemistry, Sackler School of Medicine, Tel Aviv University, Tel Aviv, Israel. ³Biological Psychiatry Laboratory Hadassah – Hebrew University Medical Center, Jerusalem, Israel. ⁴Department of Pathology, Meir Medical Center, Kfar Saba, Israel. ⁵Department of Inorganic and Physical Chemistry, Indian Institute of Science, Bangalore, India. ⁶Sackler School of Medicine, Tel Aviv University, Tel Aviv, Israel. ✉email: osnataf@gmail.com

Received: 1 June 2021 Revised: 26 August 2021 Accepted: 10 September 2021

Published online: 23 September 2021

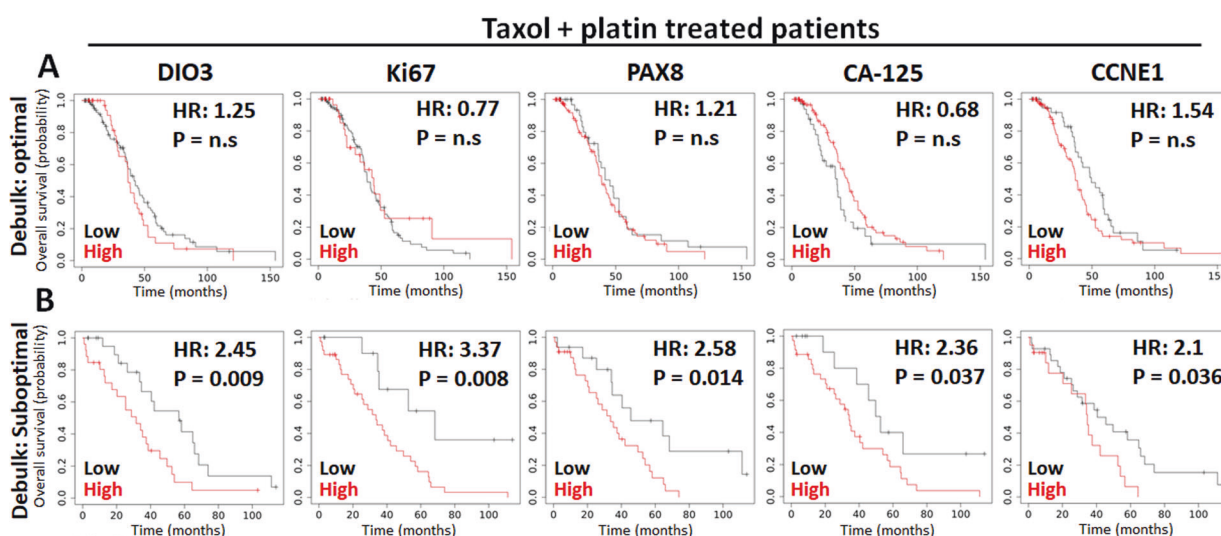


Fig. 1 Kaplan–Meier analysis for DIO3 and disease markers with overall survival in HGSOc patients. Data were retrieved from The Cancer Genome Atlas (TCGA) database using the Kaplan–Meier Plotter tool (<http://kmpplot.com>). We analyzed the gene expression level (high vs. low) for DIO3, Ki67, PAX8, CA-125, and CCNE1 in stage III HGSOc patients treated with carboplatin and taxol who underwent **A** optimal (no residual tumor) or **B** suboptimal debulking surgery. HR hazard ratio. p value <0.05 is considered significant.

using the Kaplan–Meier Plotter tool [20]. We focused on advanced stage patients (stage III) that underwent first-line treatment composed of primary debulking surgery and administration of carboplatin and taxol. Results (Fig. 1A) indicate that DIO3 expression (high vs. low) is not related to overall survival probability in patients with optimal surgery. Similar lack of association was demonstrated in this patient cohort for Ki67, PAX8, CA-125, and CCNE1, markers that are commonly elevated in HGSOc and are associated with disease progression [12]. This corresponds with the fact that successful debulking surgery in which no residual tumor is evident is the most important prognostic factor for survival [12]. When analyzing patients who underwent suboptimal procedure (Fig. 1B), a significantly higher mortality was observed for cases with high DIO3 expression (hazard ratio, HR = 2.45, $p = 0.009$). Comparable results were documented for Ki67 (HR = 3.37, $p = 0.008$), PAX8 (HR = 2.58, $p = 0.014$), CA-125 (HR = 2.36, $p = 0.037$), and CCNE1 (HR = 2.1, $p = 0.036$). Collectively, this link between DIO3 expression and survival, together with the demonstrated involvement of this enzyme in tumor proliferation, positions DIO3 as a potential target for inhibition in HGSOc.

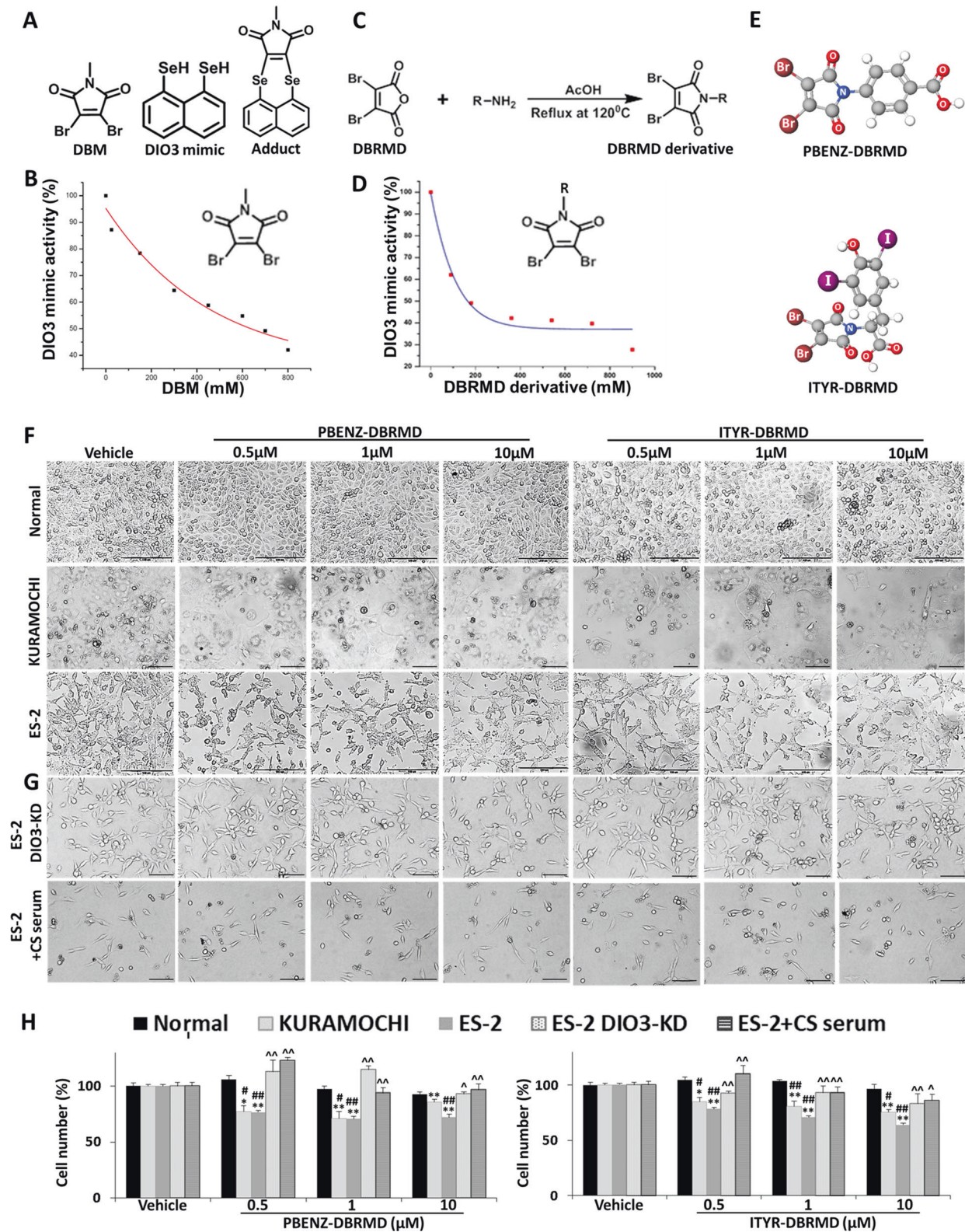
Original small compounds specifically target the DIO3 enzyme and suppress ovarian cancer growth

The DIO3 protein contains a selenium catalytic core, which is masked and inactive in its monomeric form. DIO3 becomes enzymatically active only when two monomers complex to form a homodimeric structure [21]. DIO3 main substrates, the thyroid hormones, interact with the selenol groups in the active site via their iodine atoms, resulting in iodine removal and hormone inactivation [1]. We speculated that compounds containing a bromine atom, which is a more reactive halogen than iodine, may compete with the endogenous thyroid hormones on the enzyme catalytic core. We selected dibromomaleimide (DBM) that contains two bromine atoms (Fig. 2A, left panel) and is expected to perform simultaneous nucleophilic attacks on the enzyme catalytic site. As active DIO3 protein is currently not commercially available, we assessed the inhibition capabilities of DBM using a DIO3 mimic, developed by Mugesh et al. [15–19]. This mimic contains two selenol moieties (Fig. 2A, middle panel) and behaves very similarly to the physiological DIO3 dimeric enzyme. When incubated together, the DBM molecule forms adduct with the DIO3 mimic

(Fig. 2A, right panel). We performed kinetics analysis of iodine release from the thyroid hormone substrate in the presence of DBM and the DIO3 mimic. The inhibitory plot indicated attenuated iodine release from the substrate, as a surrogate for DIO3 activity (Fig. 2B). This suggests that the bromine-containing core acts in a competitive inhibition manner. Next, we bio-conjugated a core of dibromomaleic anhydride (DBRMD) to various side chains and produced a series of novel small molecules (Fig. 2C). Kinetics studies using these novel derivatives indicated a significantly improved inhibitory potency toward the DIO3 mimic (Fig. 2D). Collectively, the drugs were designed to exclusively target cells that highly express the active DIO3 dimeric form.

We focused on the derivatives of DBRMD attached to parabenzoic acid (PBENZ-DBRMD, Fig. 2E, upper panel) or diiodotyrosine (ITYR-DBRMD, Fig. 2E, lower panel), in which the iodine atoms may further assist in increasing DIO3 specificity. These compounds underwent extensive efficacy assessment at various concentrations (0.5–10 μM , 96 h) in two DIO3-positive HGSOc cells, ES-2 and KURAMOCHI (Supplementary Fig. S1A), which highly resemble the human disease [22]. Similar to our recent work [10], we used as negative control normal ovary cells (CHOK1) that lack DIO3 expression. Microscopy images displayed lower cell density (Fig. 2F) parallel to a reduction in cell number (Fig. 2H) by both drugs in HGSOc cells, but not in DIO3-negative normal cells. Notably, while all the cell models examined express DIO1 and DIO2 (Supplementary Fig. S1B), DIO3 is exclusively expressed in the HGSOc cells. Drugs ineffectiveness in cells that are DIO3 negative, but DIO1 and DIO2 positive, proposes that the anti-proliferative effects are mediated via DIO3 inhibition and not DIO1/DIO2 inhibition. To further substantiate that the drugs mechanism of action is DIO3 specific, we examined their efficacy in the absence of the DIO3 enzyme or its substrate, T3. For that we used the DIO3 knockdown (DIO3-KD) ES-2 cells that we have previously generated [10], or ES-2 cells grown in serum deprived of the hormone. In both experimental settings, lack of efficacy was observed by microscopy (Fig. 2G) and cell number (Fig. 2H). These collective results established that the drugs are effective only when DIO3 and its substrate are present, indicating DIO3 specificity.

We next focused on ES-2, in which both DIO3 expression and the antitumor effect were greatest. By performing Annexin-PI assays, we observed induction in apoptotic cell death following



treatments (Fig. 3A). In parallel, cell cycle analysis demonstrated an elevation in Sub-G1 and a reduction in S-G2M phase (Fig. 3B). We further confirmed a potent anti-proliferative effect by PBENZ-DBRMD (Fig. 3C) and ITYR-DBRMD (Fig. 3D), using the CyQUANT cell proliferation assay. This corresponds with the known link between DIO3 and enhanced cancer proliferation [9].

DIO3-negative normal cells remained mostly unaffected. We further extracted proteins from the HGSOc cells and observed a marked reduction in a 75 kDa DIO3 band (Fig. 3E), which represents the active dimeric enzyme form, as we have previously established [10]. This reduction corresponds with the proposed mechanism of action of the compounds that were designed to

Fig. 2 Design and efficacy of novel DIO3 inhibitors in HGSOc cells. Molecular structure of **A** dibromomaleimide (DBM, left panel), DIO3 mimic (middle panel), and mimic-DBM adduct (right panel). **B** A representative inhibitory plot of the DIO3 mimic by DBM at increasing concentrations. **C** Molecular reaction of dibromomaleic anhydride (DBRMD) attachment to a side chain (R-NH₂). **D** A representative inhibitory plot of the DIO3 mimic by a modified DBRMD at increasing concentrations. **E** Molecular 3D structure of PBENZ-DBRMD (upper panel) and ITYR-DBRMD (lower panel). Bromine and iodine atoms are highlighted in brown and pink, respectively (MolView tool, <https://molview.org/>). **F** Normal ovary cells (CHOK1) and HGSOc cells (*ES-2* and KURAMOCHI) were seeded (1000 cells/96-well plates) in triplicates and treated daily with PBENZ-DBRMD and ITYR-DBRMD (0.5, 1, and 10 μM) or vehicle control (DMSO). After 96 h, cells were imaged by light microscopy (10× objective, scale bar: 100 μm). **G** *ES-2* DIO3-KD cells and *ES-2* grown in charcoal stripped (CS) serum were seeded (1000 cells/96-well plates) in triplicates and treated daily with PBENZ-DBRMD and ITYR-DBRMD (0.5, 1, and 10 μM) or vehicle control (DMSO). After 96 h, cells were imaged by light microscopy (10× objective, scale bar: 100 μm). **H** Cell number analysis (MACSQuant flow cytometer) following treatments for all cell models examined. **p* < 0.05; ***p* < 0.005, for comparing compound treated cells relative to vehicle control in each cell line. #*p* < 0.05; ##*p* < 0.005, for comparing HGSOc cells to normal control treated cells. ^*p* < 0.05; ^^*p* < 0.005, for comparing *ES-2* DIO3-KD and *ES-2*+CS serum to native *ES-2* cells. Values are mean ± STE of at least two independent experiments.

target the DIO3-dimer-expressing cells, resulting in their elimination. In parallel, a decrease in an array of central oncogenic signaling proteins, which were shown before to be repressed by T3, was shown. These include the gain-of-function R248Q-mutated p53 [23–25], as well as Pyruvate kinase 2 (PKM2), c-Myc, phosphorylated ERK (pERK), which is activated in HGSOc [26], proliferating cell nuclear antigen (PCNA), cyclin D1, and cyclin-dependent kinase 4 (CDK4). This downregulation was more pronounced in ITYR-DBRMD-treated cells. For PKM2 and c-Myc, loading control is presented in Supplementary Fig. S2. These collective in vitro results uncovered that the compounds mechanism of action is mostly anti-proliferative and confirmed that inhibition of DIO3 is a valid approach in ovarian cancer.

Effective suppression of tumor growth by the novel DIO3 inhibitors in ovarian cancer xenograft model

The toxicological profile of the novel DIO3 inhibitors, using maximal dissolved doses of PBENZ-DBRMD and ITYR-DBRMD (5 mM), was examined. The drugs or vehicle control (5% DMSO-saline) were injected intraperitoneally (IP) daily for 14 days into mice (*n* = 7 in each group). At this concentration, a high safety profile was demonstrated, with no effect on tissues morphology (Fig. 4A) or biochemical parameters (Fig. 4B). Transient behavioral effects were recorded for PBENZ-DBRMD.

We then proceeded to an efficacy experiment using the same drugs concentration (5 mM). Ovarian cancer xenograft model was generated by subcutaneous (SC) injections of *ES-2* cells into the left flank of female nude mice. Eleven days after inoculation, mice were randomized into three groups (*n* = 6) and treated by IP injections (5 days a week for 3 weeks) of PBENZ-DBRMD or ITYR-DBRMD in comparison to vehicle control (5% DMSO-PBS). During the experimental period, no change in body weight was detected in the study cohort (Supplementary Fig. S3). Results indicated a substantial inhibition in the average tumor volume throughout the study period by PBENZ-DBRMD and a more pronounced cytostatic effect by ITYR-DBRMD (Fig. 4C). These results were compatible with smaller tumor size (Fig. 4D) and lower tumor weight (Fig. 4E) at study end. Tumor weights were with borderline significance for PBENZ-DBRMD (*p* = 0.054) and statistical significance for ITYR-DBRMD (*p* = 0.02). The collected tumors were further examined for an array of oncogenes and proliferation markers by western blot (WB) analysis (Fig. 4F). A significant reduction in β-catenin, a central player in epithelial to mesenchymal transition with a known function in ovarian cancer [27], the Müllerian marker PAX8 [28], mutated p53, PCNA, Cyclin D1, and CDK4, was documented in mice treated with PBENZ-DBRMD or ITYR-DBRMD, corresponding with lower tumor size and mitotic rate. The tumor tissues underwent additional analysis by histological (H&E) and IHC examination for DIO3 and the common proliferation marker Ki67 (Fig. 4G). Results indicate that the high expression of membranal DIO3 enzyme and Ki67 staining in untreated tumors is significantly diminished following treatment with the drugs. We further assessed whether the two compounds,

which inhibit T3 degradation by DIO3, may alter free T3 serum levels. We did not observe such a systemic effect, suggesting that the drugs act locally in tumor-specific regions (Fig. 4H).

DIO3-silenced tumors are unaffected by the inhibitors, confirming target specificity in vivo

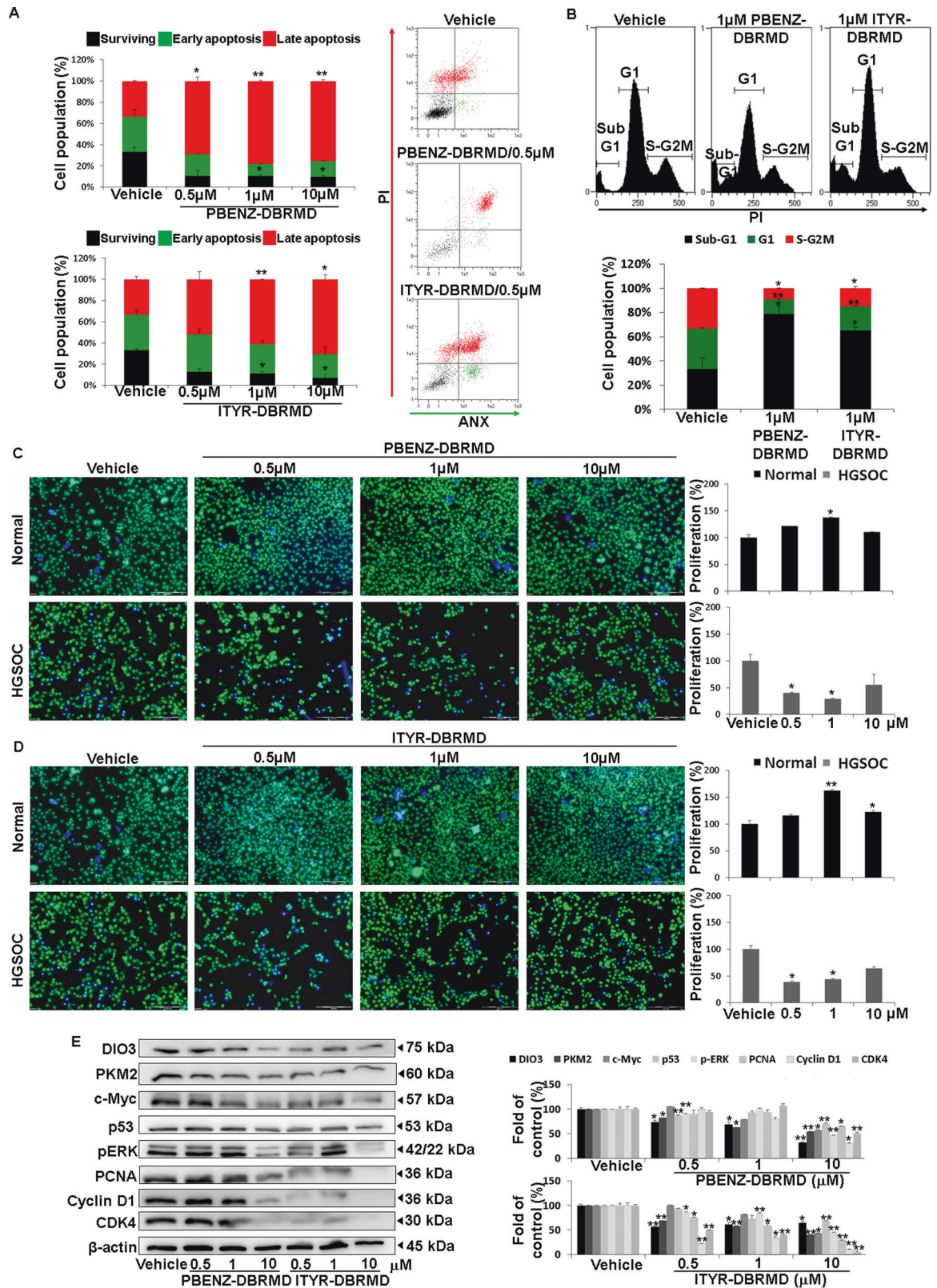
Following the observation that PBENZ-DBRMD and ITYR-DBRMD effectively suppress HGSOc tumor growth in vitro and in vivo, we were interested to validate that these effects are mediated via DIO3 inhibition. Ineffectiveness of both drugs in the absence of DIO3 would provide such indirect target validation in vivo. To that end, we used the DIO3-KD *ES-2* cells, which displayed stable DIO3 silencing in xenograft mice, as we recently reported [10]. We inoculated the DIO3-KD cells into the right flank of female nude mice, which were treated following randomization for 3 weeks with the two DIO3 inhibitors or vehicle control (5% DMSO-PBS). Results show that both PBENZ-DBRMD and ITYR-DBRMD did not inhibit the average tumor volume, throughout the study period, compared with the vehicle-treated mice (Fig. 5A). Similarly, at study end, tumor size (Fig. 5B) and weight (Fig. 5C) were indistinguishable from the vehicle-treated tumors. We further confirmed that in comparison to DIO3-positive tumors, DIO3 remained silenced at study end in the DIO3-KD tumors, as shown by IHC (Fig. 5D) and WB analysis (Fig. 5E). Collectively, ineffectiveness of the compounds in DIO3-depleted tumors, in contrast to their potency in DIO3-expressing HGSOc tumors, provides further support that DIO3 is their specific enzyme target.

DISCUSSION

Accumulating evidence suggests that the T3 catabolizing enzyme, DIO3, is highly expressed in several neoplastic tissues and is involved in tumorigenesis [2, 29]. The reactive selenol group in the enzyme catalytic site leads to inactivation of T3 and its tumor-suppressive actions, thus facilitating cancer proliferation. Together with the fact that DIO3 is hardly expressed in healthy adult tissues [9], positions this enzyme as an attractive target for inhibition in oncology. Such DIO3 inhibition will increase T3 bioavailability and contribute to tumor regression. Although targeting DIO3 in cancer may potentially serve as a promising treatment approach, to the best of our knowledge there are no specific DIO3 inhibitors available.

To understand the structural requirements for DIO3 inhibition, we utilized a synthetic DIO3 mimic [15–19] and developed a series of first-in-class bromine-containing DIO3 inhibitors. Some of our compounds were modified by adding another halogen atom, iodine, which further stabilizes their bonding at the enzyme active site, and may produce greater DIO3 specificity. Such introduction of halogen atoms, including bromine, is commonly employed in drug design [30, 31] with several dozens of bromo-derivative drugs already approved for use in various pathological conditions in humans, including oncology [32–36].

Efficacy of our compounds was examined in ovarian cancer, a highly aggressive disease with a need for novel treatment



approaches. The recently established role for DIO3 in this malignancy [10], together with its correlation with patients' survival, suggests a potential for DIO3 inhibition in ovarian cancer. In this preclinical work we present significant antitumor effects by two best hit DIO3 inhibitors, PBENZ-DBRMD and ITYR-DBRMD

in HGSOc cell lines. Following confirmation of a high safety profile for the drugs, we observed targeted elimination of DIO3-positive proliferating cancer cells and a significant tumor inhibition in ovarian cancer xenografts, resulting in a near cytostatic effect. These tumor-suppressive effects are mediated by a decrease in a

Fig. 3 Induction of apoptosis and attenuation of cell proliferation and T3-related proteins in HGSOc cells treated with the DIO3 inhibitors. HGSOc ES-2 cells were seeded (1000 cells/96-well plates) in triplicates and treated daily with PBENZ-DBRMD and ITYR-DBRMD (0.5, 1, and 10 μ M) or vehicle control (DMSO). After 96 h, cells underwent analysis by flow cytometry for **A** Annexin (ANX)-PI. Percentages of surviving cells (Annexin-/PI-), early apoptosis (Annexin+/PI-), and late apoptosis (Annexin+/PI+) are presented in the left panel. Representative histograms of 0.5 μ M are shown in the right panel. **B** Cell cycle. Representative histograms for 1 μ M are shown in the upper panel and percentages of Sub-G1, G1, and S-G2M are presented in the lower panel. Next, normal ovary and ES-2 HGSOc cells were seeded (1000 cells/96-well plates) in triplicates and treated daily with **C** PBENZ-DBRMD and **D** ITYR-DBRMD (0.5, 1, and 10 μ M) or vehicle control (DMSO). After 96 h, the cells were assessed using the CyQuant proliferation assay. Proliferating cells are stained green and the nucleus in blue (10 \times objective, scale bar: 100 μ m). Proliferation quantifications as fold of control are presented in the right panels. **E** 1×10^5 ES-2 cells were seeded in 24-well plates and treated daily with PBENZ-DBRMD, ITYR-DBRMD (0.5, 1, and 10 μ M), or vehicle control (DMSO). After 96 h, total proteins were extracted and analyzed by WB for DIO3 and the oncogenic signaling proteins PKM2, c-Myc, gain-of-function-mutated p53, pERK, PCNA, Cyclin D1, and CDK4. β -actin was used as a loading control. For PKM2 and c-Myc, loading control is presented in Supplementary Fig. S2. Quantification of normalized bands intensity as fold of control is presented in the right panel. All experiments are representative of at least two independent repeats. Values are mean \pm STE, * $p < 0.05$, ** $p < 0.005$.

panel of pro-mitogenic proteins, such as the gain-of-function-mutated form of p53 [23–25]. Moreover, the treated tumors displayed reduced levels of the proliferation marker Ki67, as well as PAX8, an ovarian cancer marker that was shown to be directly linked with mitogenesis [28]. Notably, the DIO3 inhibitors that were designed to attenuate T3 catabolism by the enzyme did not produce a systemic effect on T3 circulating levels, indicating that the drugs act locally inside the tumor region.

Support that the novel compounds target DIO3 and not the other two deiodinase family members, DIO1 and DIO2, is the drugs ineffectiveness in normal cells, which are positive only for DIO1 and DIO2. In addition, we have strong experimental evidence that silencing or inhibiting DIO1 results in the induction of proliferation, while overexpressing DIO1 attenuates HGSOc cell growth (unpublished data). These results are opposite to the anti-proliferative outcome following DIO3 inhibition. Therefore, if our drugs were acting as DIO1 or DIO2 inhibitors, an opposite effect would have been anticipated. Moreover, in contrast to the high efficiency of the compounds in DIO3-positive HGSOc cells and xenografts, DIO3-depleted tumors remained unaffected. Lastly, lack of efficacy by these drugs under DIO3-negative or T3-depleted conditions also suggests that their mechanism of action is mediated via attenuating T3 catabolism. This is further supported by the downregulation in an array of proliferation-related proteins, which were shown before to be repressed by T3. These include pERK [37–40], PCNA [41], and c-Myc [5, 42], the latter contains negative T3 responsive elements [43, 44]. A comparable reduction by T3 was reported for cyclin D1 [5, 6, 42], another T3-repressed target-gene [45, 46], which together with CDK4 governs cell cycle progression. Moreover, we observed a reduction in PKM2, which facilitates aerobic glycolytic and is known to be allosterically inhibited by T3 [47]. These collective data strongly suggest that the drugs anti-proliferative effects are mediated via targeting the DIO3 enzyme, increasing T3 bioavailability.

In summary, DIO3 scavenges the thyroid hormone T3 and facilitates tumor growth (Fig. 6, left panel), as we have established in ovarian cancer models [10]. Our newly developed small compounds interact with the catalytic site in the DIO3 dimer and prevent T3 catabolism. This leads to induction in apoptosis and a significant reduction in T3-related target genes with known roles in cancer proliferation, resulting in tumor suppression (Fig. 6, right panel). This novel therapeutic paradigm with a defined target is expected to portray tumor-specific effects in ovarian cancer and potentially other types of DIO3-dependent malignancies.

MATERIALS AND METHODS

TCGA analysis

Analysis of the expression of DIO3, Ki67, PAX8, CA-125, and CCNE1 and clinical information on HGSOc patients were extracted from TCGA database using the Kaplan–Meier Plotter tool [20].

Reagents and antibodies

All reagents, including T3 hormone, were obtained from Sigma Aldrich (St. Louis, MO, USA). Primary antibodies are detailed in Supplementary Table S1.

Synthesis of the small compound DIO3 inhibitors

2, 3-Dibromomaleic anhydride (DBRMD). In a pressure-resistant sealed tube, maleic anhydride (1 g, 10.20 mmol), catalytic amount of aluminum chloride (0.023 g, 0.18 mmol), and bromine (1.05 mL, 20.4 mmol, 2 eq.) were heated to 1200 C for 16 h. On cooling to room temperature, the mixture was taken up in ethyl acetate and concentrated in vacuo to give 2, 3-dibromomaleic anhydride as solid (yield = 90%).

N-(p-Benzoic acid)-2, 3-dibromo-maleimide (PBENZ-DBRMD). In a round bottom flask, 2, 3-dibromomaleic anhydride (500 mg, 1.95 mmol, 1 eq) and para-amino benzoic acid (PBENZ, 320 mg, 2.32 mmol, 1.2 eq) were mixed with acetic acid (15 mL) and heated at 1200 C with stirring for 8 h. After that, the mixture was allowed to cool down to room temperature and filtered. The residue was washed with methanol and methylene chloride for three times and dried to afford yellow solid powder (yield = 75%). The molecular weight of PBENZ-DBRMD is 375.

Diiodotyrosine-2, 3-dibromo-maleimide derivative (ITYR-DBRMD). To a solution of 2, 3-dibromomaleic anhydride (500 mg, 1.95 mmol, 1 eq) in acetic acid (15 mL) diiodotyrosine (ITYR, 1.26 g, 2.92 mmol, 1.5 eq) was added and the mixture was heated at 1200 C for 12 h. Next, the mixture was allowed to cool down to room temperature. Solvent was removed under reduced pressure. The product was extracted with ethyl acetate (three times) and washed with brine solution. The ethyl acetate layer was then evaporated and purified by column chromatography by using 50% petroleum ether and ethyl acetate as eluent to give solid product (yield = 52%). The molecular weight of ITYR-DBRMD is 671. Structure and purity of both PBENZ-DBRMD and ITYR-DBRMD were confirmed by 1 H NMR spectroscopy and HPLC. The NMR spectra of the compounds after column purification show content and purity (Supplementary Fig. S4). The purity was further assessed by reverse-phase HPLC method (Lichrospher, C18 column, 4.6 \times 250 mm, 5 μ m) with isocratic elution using acetonitrile/water as the mobile phase. The formation of product was monitored at 254/275 nm. The compounds percentage of purity was 97–98%, as calculated by comparing peak areas (Supplementary Fig. S5). Compounds were dissolved to 100 mM stock solution in DMSO and kept at –20 until use.

DIO3 mimic inhibition

The DIO3 mimic was freshly prepared by reducing the diselenides by NaBH₄ prior to use. The final assay mixture contained 600 μ M of the mimic, 300 μ M of T₄, and 10 mM of DTT. The deiodination reactions were carried out in 100 mM phosphate buffer (pH 7.5). The reaction mixture was incubated at 37 $^\circ$ C in 1.5 mL sample vial. The reaction products were analyzed by a reverse-phase HPLC method. The HPLC experiments were carried out on a Waters Alliance System (Milford, MA) consisting of a 2695 separation module, a 2996 photodiode-array detector, and a fraction collector. A built-in autosampler was used for sample injection. The Alliance HPLC System was controlled with EMPOWER software (Waters Corporation, Milford, MA). The samples were eluted on a Lichrosphere C18 column, (4.6 μ , 150 mm, 5 mm) with gradient elution

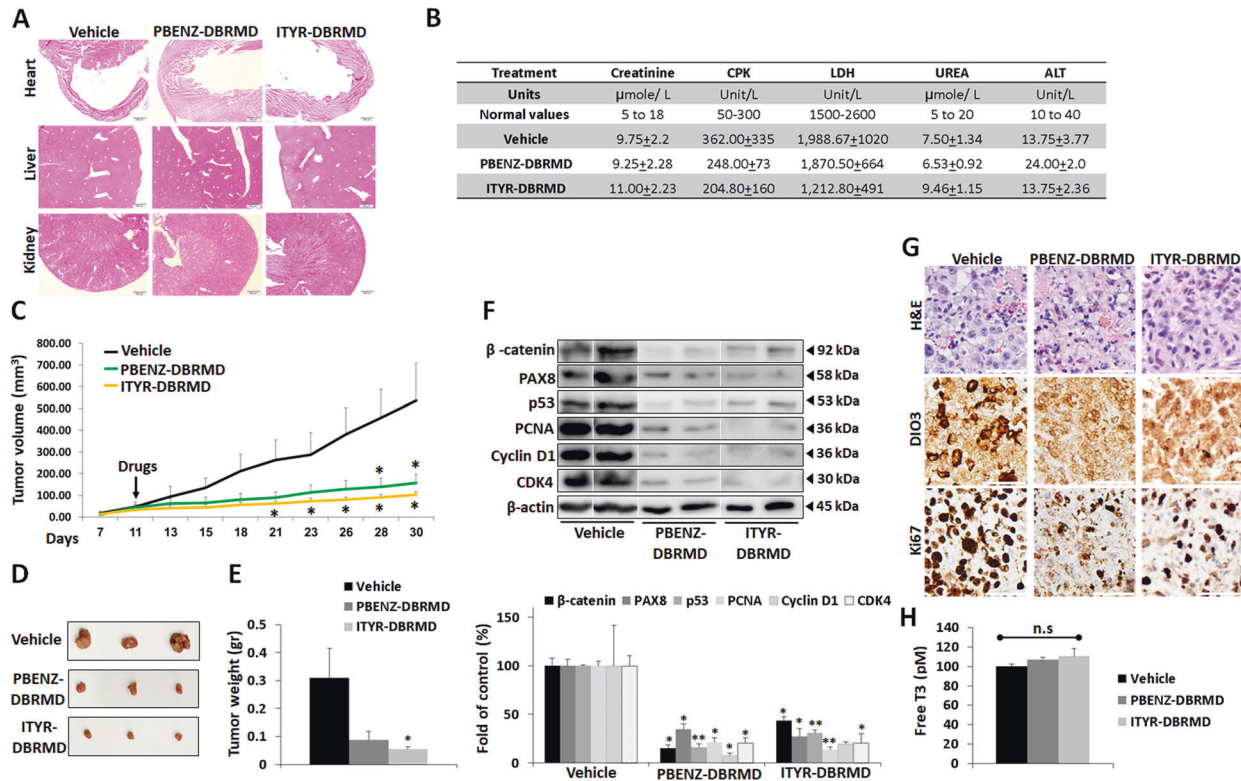


Fig. 4 DIO3 inhibitors suppress tumor growth in HGSOX xenograft model. Toxicology studies of PBENZ-DBRMD and ITYR-DBRMD compared to vehicle. **A** Representative images of H&E staining from liver, heart, and kidneys. All samples underwent pathological examination and were defined as unremarkable. **B** Blood samples obtained at sacrifice were examined for the following biochemical parameters in 4–5 mice per treatment group: creatinine, CPK, LDH, urea, and ALT. The table shows mean values for each treatment group. Next, 1×10^6 HGSOX cells (*ES-2*) were injected SC into the flank of athymic nude mice ($n = 18$). Mice were randomized into three treatment groups ($n = 6$) and starting on day 11 treated daily with PBENZ-DBRMD, ITYR-DBRMD, or vehicle control for 3 weeks. **C** Average tumor volume during the experimental period. **D** Representative excised tumors at study end. **E** Average tumor weight at study end. **F** Total proteins were extracted from tumors treated with vehicle, PBENZ-DBRMD, or ITYR-DBRMD and evaluated by WB for β -catenin, PAX8, p53, PCNA, Cyclin D1, and CDK4. β -actin was used as a loading control. For each treatment, results from two representative tumors are presented. Skipping lanes are clearly marked by a separating line. Quantification of normalized bands intensity as fold of control is presented in the lower panel. **G** H&E and IHC staining for DIO3 and Ki67 in representative FFPE tumors from mice treated with vehicle, PBENZ-DBRMD, or ITYR-DBRMD. Objective 10 \times , scale bar: 50 μM . **H** Serum free T3 levels measurements at the end of the in vivo study. n.s. nonsignificant. Values are mean \pm STE, * $p < 0.05$. ** $p < 0.005$.

using acetonitrile/ammonium acetate (pH 4.0) as the mobile phase. The formation of rT3 was monitored at $\lambda = 275$ nm, and the amounts of deiodinated products formed in the reactions were calculated by comparing the peak areas.

Cell cultures

HGSOX *ES-2* and KURAMOCHI cells were provided by Dr Ruth Perets (Rambam Medical Center, Haifa, Israel). Chinese hamster normal ovary cells (CHOK1) were a kind gift from Prof. Philippe Cl'ezardin (University of Lyon, Lyon, France). Cells were grown in RPMI1640 medium (Biological Industries, Beit Haemek, Israel) supplemented with 10% heat-inactivated FBS and 1% penicillin-streptomycin antibiotics. The culture media was validated to contain physiological thyroid hormone levels. For T3-deficient medium, the cells were grown in 10% charcoal stripped serum that is depleted for thyroid hormones (Biological Industries). STR/mutation profiling was used for authentication and mycoplasma was screened periodically.

Generation of DIO3 knockdown (DIO3-KD) cells

ES-2 cells were seeded ($0.5 \times 10^6/6$ well plates) and stably transfected with a pool of three human DIO3 shRNA plasmids (sc-77150-SH) or a nonspecific scrambled control shRNA plasmids (sc-108060), from Santa Cruz Technologies (Dallas, TX, USA). Transfections were performed following manufacturer's instructions with shRNA transfection reagent (Santa Cruz). After selection with puromycin and clones isolation, successful stable inhibition was confirmed at the RNA (Real-time PCR) and protein levels (WBs) as previously performed [10].

Microscopy

Images were obtained by a microscope equipped with a camera with Olympus model BX41 for IHC slides and model IX71 for cell cultures (Olympus, Tokyo, Japan). Analysis was performed by cellSens Entry Olympus imaging software.

Flow cytometry (FC)

Absolute cell counts, cell cycle, and Annexin V/Propidium Iodide (Annexin-PI) were performed using MACSQuant flow cytometer (Miltenyi Biotec, Bergisch Gladbach, Germany), as detailed before [48, 49]. For DIO1-3 expression, cells were permeabilized and labeled with a fluorescently-conjugated DIO1-3 antibodies.

CyQUANT cell proliferation assay

ES-2 and CHOK1 cells were seeded in triplicates (1×10^3 cells/96-well plates) and treated daily with 0.5, 1, and 10 μM of the DIO3 inhibitors compared to vehicle control (DMSO). After 96 h, CyQuant cell proliferation assay kit (Invitrogen, Thermo Fisher Scientific, Waltham, MA, USA) was used, following the manufacturer's instructions. Green fluorescent dye represents proliferating cells. Nucleus was stained blue with Hoechst 33342 (Molecular probes, Eugene, OR, USA) and microscopy images were obtained.

Western blots (WB)

Total proteins were extracted from cell lines or homogenized tumor tissues and separated on 10–12.5% polyacrylamide gels, fast-transferred to PVDF

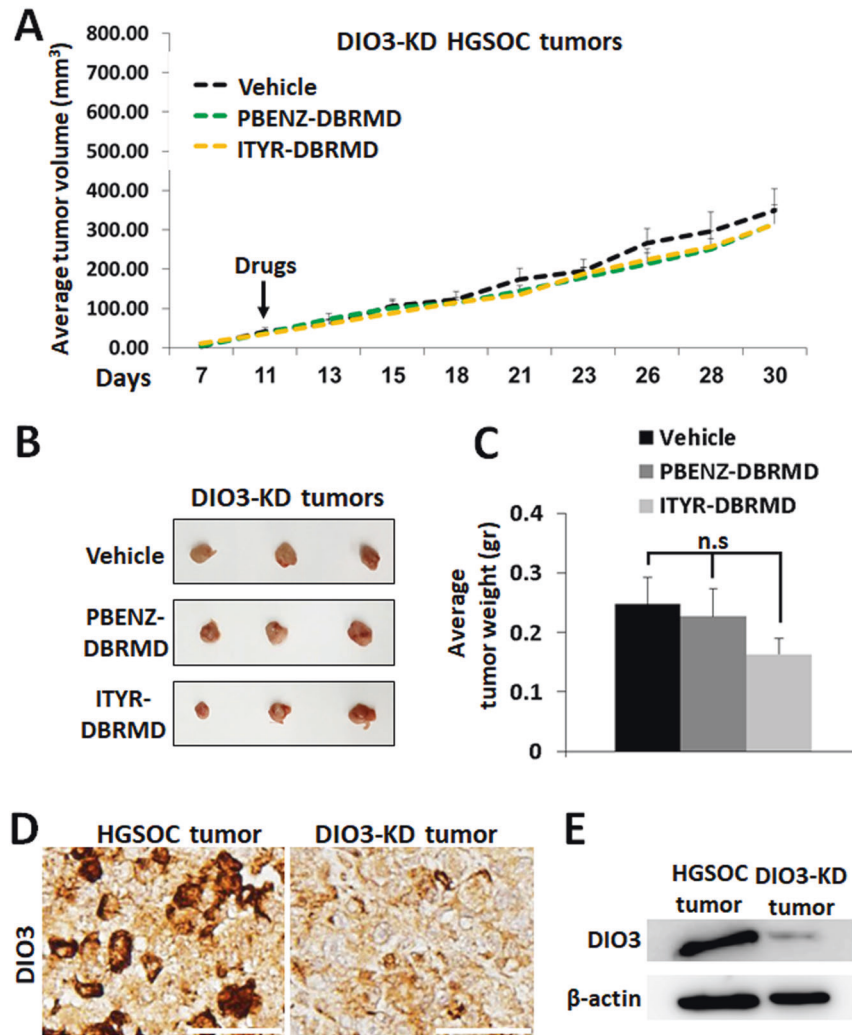


Fig. 5 **DIO3-silenced tumors are unaffected by the drugs.** **A** DIO3-KD cells (1×10^6) were injected SC into the flank of athymic nude mice ($n = 18$). Mice were randomized into three treatment groups ($n = 6$) and starting on day 11 treated daily with 5 mM PBENZ-DBRMD, ITYR-DBRMD, or vehicle control for 3 weeks. Average tumor volume during the experimental period is presented. **B** Representative excised tumors at study end. **C** Average tumor weight at study end. Values are mean \pm STE. **D** HGSOC tumors generated by SC inoculation of DIO3 knockdown (DIO3-KD) ES-2 cells display stable DIO3 silencing in representative xenograft mice by IHC (objective 10 \times , scale bar: 50 μ m) and **E** WB analysis, in comparison to DIO3-positive HGSOC tumor. β -actin was used as a loading control.

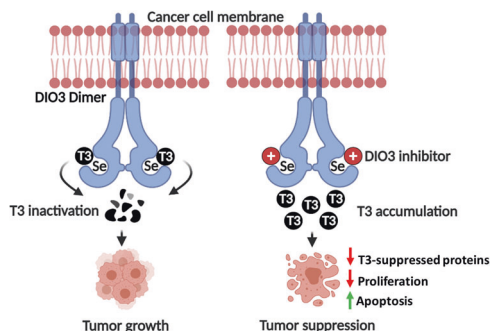


Fig. 6 **Illustration of DIO3 enzymatic activity and inhibition in cancer cells.** The DIO3 dimer localizes at the cell membrane and via its selenium-containing catalytic core inactivates T3 and its tumor-suppressive actions, facilitating cancer proliferation. Inhibition of DIO3 using small compounds that interact with the catalytic site in the DIO3 dimer results in endogenous T3 accumulation, leading to a reduction in T3-suppressed proteins and cell proliferation, induction in apoptosis, and, eventually, tumor suppression.

membranes, and analyzed by WB using specific primary antibodies. Bound antibodies were visualized using horseradish peroxidase-conjugated secondary antibodies goat anti-Rabbit IgG (Jackson ImmunoResearch Laboratories, West Grove, PA, USA), followed by enhanced chemiluminescence detection kit (PIERCE, Thermo Fisher Scientific, Bremen, Germany). Integrated optical densities of the bands were measured by Las3000 imaging system, analyzed by Multi-gauge v3.0 software (Fujifilm Life Science, Tokyo, Japan) and normalized to β -actin.

Toxicology studies

Balb/C mice (Envigo, Rehovot, Israel) were used for the toxicology experiment, which was conducted at the Biological Psychiatry Laboratory Hadassah-Hebrew University Medical Center, Jerusalem, Israel, according to protocols approved by the institution Animal Care and Use Committee. The mice were housed in a temperature-controlled environment with a regular light/dark cycle. Food and water were freely available. Maximal doses of PBENZ-DBRMD and ITYR-DBRMD were selected based on their solubility in 5% DMSO-saline vehicle. PBENZ-DBRMD was administered at a concentration of 18.5 mg/kg body weight in vehicle (5 mM) and ITYR-DBRMD at 33.5 mg/kg body weight in vehicle (5 mM). The compounds or vehicle ($n = 7$ mice for each group) were injected IP daily for 14 days using sterile syringes. Each solution was administered in a volume of 0.1 mL per

10 g of animal body weight. Observations of drug effects on general health and behavior commenced immediately after injections and continued for 30 min and thereafter every half an hour for 5 min over a period of 6 h. After termination of the observational test battery, animals were sacrificed by IP injection of veterinary pentol (13.3 mg/kg animal body weight) and cardiac blood was drawn for biochemistry. The abdominal cavity was opened and liver, heart, and kidneys were removed for pathological evaluation.

HGSOC xenograft model

The study was outsourced (Almog Diagnostic LTD, Shoham, Israel) and performed in compliance with the recommendations of the Guide for Care and Use of Laboratory Animals and following Helsinki approval. Nine-week-old female athymic nude mice ($n = 18$, Envigo, Ness-Ziona, Israel) were SC injected with scrambled control ES-2 cells and DIO3-knockdown (DIO3-KD) ES-2 cells (1×10^6 cells each) into the left and right flanks, respectively. After 11 days in which the tumors were allowed to grow, mice were randomized into three groups (6 mice/group) and treated with equimolar (5 mM) amounts of PBENZ-DBRMD (18.5 mg/kg) and ITYR-DBRMD (33.5 mg/kg) or with the vehicle control (5% DMSO-PBS) by IP injection for 5 days a week for a period of 3 weeks. Tumor growth and mice weight were measured twice a week. Tumor volume was estimated according to the following formula: length \times (width)²/2. Outlier tumors were excluded from analysis. At study end (30 days) the tumors were weighted and collected for protein extractions or FFPE preparations and blood was collected for assessing free T3 (FT3) levels.

Immunohistochemistry (IHC)

Staining was done using specific antibodies on a Ventana Benchmark XT automatic stainer (Ventana, Tucson, Arizona, USA).

Free T3 (FT3) serum levels

FT3 levels were measured using the Elecsys FT3 III assay on cobas e 411 analyzer in Meir Medical Center endocrinology laboratory (normal range 3.1–6.8 pmol/L).

Statistical analysis

Experiments were repeated independently in duplicates or triplicates and analyzed by two-sided unpaired *t*-test or by ANOVA for multiple comparisons. Significance was determined at $p < 0.05$. Results are presented as mean \pm STE.

REFERENCES

- Luongo C, Dentice M, Salvatore D. Deiodinases and their intricate role in thyroid hormone homeostasis. *Nat Rev Endocrinol*. 2019;15:479–88.
- Goemann IM, Marczyk VR, Romitti M, Wajner SM, Maia AL. Current concepts and challenges to unravel the role of iodothyronine deiodinases in human neoplasias. *Endocr Relat Cancer*. 2018;25:R625–R645.
- Goemann IM, Romitti M, Meyer ELS, Wajner SM, Maia AL. Role of thyroid hormones in the neoplastic process: an overview. *Endocr Relat Cancer*. 2017;24:R367–R385.
- Catalano V, Dentice M, Ambrosio R, Luongo C, Carollo R, Benfante A, et al. Activated thyroid hormone promotes differentiation and chemotherapeutic sensitization of colorectal cancer stem cells by regulating Wnt and BMP4 signaling. *Cancer Res*. 2016;76:1237–44.
- Dentice M, Luongo C, Ambrosio R, Sibilio A, Casillo A, Iaccarino A, et al. beta-Catenin regulates deiodinase levels and thyroid hormone signaling in colon cancer cells. *Gastroenterology*. 2012;143:1037–47.
- Dentice M, Luongo C, Huang S, Ambrosio R, Elefante A, Mirebeau-Prunier D, et al. Sonic hedgehog-induced type 3 deiodinase blocks thyroid hormone action enhancing proliferation of normal and malignant keratinocytes. *Proc Natl Acad Sci USA*. 2007;104:14466–71.
- Di Girolamo D, Ambrosio R, De Stefano MA, Mancino G, Porcelli T, Luongo C, et al. Reciprocal interplay between thyroid hormone and microRNA-21 regulates hedgehog pathway-driven skin tumorigenesis. *J Clin Invest*. 2016;126:2308–20.
- Romitti M, Wajner SM, Ceolin L, Ferreira CV, Ribeiro R, Rohenkohl HC, et al. MAPK and SHH pathways modulate type 3 deiodinase expression in papillary thyroid carcinoma. *Endocr Relat Cancer*. 2016;23:135–46.
- Nappi A, De Stefano MA, Dentice M, Salvatore D. Deiodinases and cancer. *Endocrinology*. 2021;162:bqab016.
- Moskovich D, Alfandari A, Finkelshtein Y, Weisz A, Katzav A, Kidron D, et al. DIO3, the thyroid hormone inactivating enzyme, promotes tumorigenesis and metabolic reprogramming in high grade serous ovarian cancer. *Cancer Lett*. 2021;501:224–33.
- Siegel RL, Miller KD, Fuchs HE, Jemal A. *Cancer Statistics, 2021*. *CA Cancer J Clin*. 2021;71:7–33.
- Lheureux S, Gourley C, Vergote I, Oza AM. Epithelial ovarian cancer. *Lancet*. 2019;393:1240–53.
- Renko K, Schäche S, Hoefig CS, Welsink T, Schwiebert C, Braun D, et al. An improved nonradioactive screening method identifies genistein and xanthohumol as potent inhibitors of iodothyronine deiodinases. *Thyroid*. 2015;25:962–8.
- Steebhorn C, Schweizer U. Structure and mechanism of iodothyronine deiodinases—what we know, what we don't know, and what would be nice to know. *Exp Clin Endocrinol Diabetes*. 2020;128:375–8.
- Manna D, Mughesh G. A chemical model for the inner-ring deiodination of thyroxine by iodothyronine deiodinase. *Angew Chem Int Ed*. 2010;49:9246–9.
- Manna D, Mughesh G. Deiodination of thyroid hormones by iodothyronine deiodinase mimics: does an increase in the reactivity alter the regioselectivity? *J Am Chem Soc*. 2011;133:9980–3.
- Manna D, Mughesh G. Regioselective deiodination of thyroxine by iodothyronine deiodinase mimics: an unusual mechanistic pathway involving cooperative chalcogen and halogen bonding. *J Am Chem Soc*. 2012;134:4269–79.
- Mondal S, Mughesh G. Biomimetic deiodination of thyroid hormones and iodothyronamines—a structure–activity relationship study. *Org Biomolecular Chem*. 2016;14:9490–9500.
- Raja K, Mughesh G. Remarkable effect of chalcogen substitution on an enzyme mimetic for deiodination of thyroid hormones. *Angew Chem Int Ed*. 2015;54:7674–8.
- Györfy B, Lániczky A, Szállási Z. Implementing an online tool for genome-wide validation of survival-associated biomarkers in ovarian-cancer using microarray data from 1287 patients. *Endocr Relat Cancer*. 2012;19:197–208.
- Schweizer U, Schlicker C, Braun D, Köhrle J, Steebhorn C. Crystal structure of mammalian selenocysteine-dependent iodothyronine deiodinase suggests a peroxidase-like catalytic mechanism. *Proc Natl Acad Sci USA*. 2014;111:10526–31.
- Domcke S, Sinha R, Levine DA, Sander C, Schultz N. Evaluating cell lines as tumour models by comparison of genomic profiles. *Nat Commun*. 2013;4:2126.
- Yaginuma Y, Westphal H. Abnormal structure and expression of the p53 gene in human ovarian carcinoma cell lines. *Cancer Res*. 1992;52:4196–9.
- Bargonetti J, Prives C. Gain-of-function mutant p53: history and speculation. *J Mol Cell Biol*. 2019;11:605–9.
- Cole AJ, Dwight T, Gill AJ, Dickson K-A, Zhu Y, Clarkson A, et al. Assessing mutant p53 in primary high-grade serous ovarian cancer using immunohistochemistry and massively parallel sequencing. *Sci Rep*. 2016;6:1–12.
- Simpkins F, Jang K, Yoon H, Hew KE, Kim M, Azzam DJ, et al. Dual Src and MEK inhibition decreases ovarian cancer growth and targets tumor initiating stem-like cells. *Clin Cancer Res*. 2018;24:4874–86.
- Nguyen VHL, Hough R, Bernaudo S, Peng C. Wnt/ β -catenin signalling in ovarian cancer: Insights into its hyperactivation and function in tumorigenesis. *J Ovarian Res*. 2019;12:1–17.
- Ghannam-Shahbari D, Jacob E, Kakun RR, Wasserman T, Korsensky L, Sternfeld O, et al. PAX8 activates a p53-p21-dependent pro-proliferative effect in high grade serous ovarian carcinoma. *Oncogene*. 2018;37:2213–24.
- Dentice M, Antonini D, Salvatore D. Type 3 deiodinase and solid tumors: an intriguing pair. *Expert Opin Ther Targets*. 2013;17:1369–79.
- Hernandes MZ, Cavalcanti SMT, Moreira DRM, de Azevedo Junior WF, Leite ACL. Halogen atoms in the modern medicinal chemistry: hints for the drug design. *Curr Drug Targets*. 2010;11:303–14.
- Wilcken R, Zimmermann MO, Lange A, Joerger AC, Boeckler FM. Principles and applications of halogen bonding in medicinal chemistry and chemical biology. *J Med Chem*. 2013;56:1363–88.
- Kopetz S, Grothey A, Yaeger R, Van Cutsem E, Desai J, Yoshino T, et al. Encorafenib, binimetinib, and cetuximab in BRAF V600E-mutated colorectal cancer. *N Engl J Med*. 2019;381:1632–43.
- Dhillon S. Lonafarnib: first approval. *Drugs*. 2021;81:283–9.
- Smith BD, Kaufman MD, Lu W-P, Gupta A, Leary CB, Wise SC, et al. Ripretinib (DCC-2618) is a switch control kinase inhibitor of a broad spectrum of oncogenic and drug-resistant KIT and PDGFRA variants. *Cancer Cell*. 2019;35:738–51.e739.
- Andrea VR. The role of halogen bonding in inhibitor recognition and binding by protein kinases. *Curr Top Med Chem*. 2007;7:1336–48.
- Wasik R, Łębska M, Felczak K, Poznański J, Shugar D. Relative role of halogen bonds and hydrophobic interactions in inhibition of human protein kinase CK2 α by tetrabromobenzotriazole and some C (5)-substituted analogues. *J Phys Chem B*. 2010;114:10601–11.
- Contreras-Jurado C, Alonso-Merino E, Saiz-Ladera C, Valiño AJ, Regadera J, Alemany S, et al. The thyroid hormone receptors inhibit hepatic interleukin-6 signaling during endotoxemia. *Sci Rep*. 2016;6:1–12.

38. Suarez J, Scott BT, Suarez-Ramirez JA, Chavira CV, Dillmann WH. Thyroid hormone inhibits ERK phosphorylation in pressure overload-induced hypertrophied mouse hearts through a receptor-mediated mechanism. *Am J Physiol Cell Physiol*. 2010;299:C1524–C1529.
39. Flores-Morales A, Gullberg H, Fernandez L, Ståhlberg N, Lee NH, Vennström B, et al. Patterns of liver gene expression governed by TR β . *Mol Endocrinol*. 2002;16:1257–68.
40. García-Silva S, Aranda A. The thyroid hormone receptor is a suppressor of ras-mediated transcription, proliferation, and transformation. *Mol Cell Biol*. 2004;24:7514–23.
41. Punchihewa C, Inoue A, Hishiki A, Fujikawa Y, Connelly M, Evison B, et al. Identification of small molecule proliferating cell nuclear antigen (PCNA) inhibitor that disrupts interactions with PIP-box proteins and inhibits DNA replication. *J Biol Chem*. 2012;287:14289–300.
42. Perez-Juste G, Aranda A. The cyclin-dependent kinase inhibitor p27Kip1 is involved in thyroid hormone-mediated neuronal differentiation. *J Biol Chem*. 1999;274:5026–31.
43. Pérez-Juste G, García-Silva S, Aranda A. An element in the region responsible for premature termination of transcription mediates repression of c-myc gene expression by thyroid hormone in neuroblastoma cells. *J Biol Chem*. 2000;275:1307–14.
44. Gagne R, Green JR, Dong H, Wade MG, Yauk CL. Identification of thyroid hormone receptor binding sites in developing mouse cerebellum. *BMC Genomics*. 2013;14:1–14.
45. Nappi A, Murolo M, Sagliocchi S, Miro C, Cicatiello AG, Di Cicco E, et al. Selective inhibition of genomic and non-genomic effects of thyroid hormone regulates muscle cell differentiation and metabolic behavior. *Int J Mol Sci*. 2021;22:7175.
46. Porlan E, Vidaurre OG, Rodríguez-Peña A. Thyroid hormone receptor- β (TR β 1) impairs cell proliferation by the transcriptional inhibition of cyclins D1, E and A2. *Oncogene*. 2008;27:2795–800.
47. Cheng SY, Leonard JL, Davis PJ. Molecular aspects of thyroid hormone actions. *Endocr Rev*. 2010;31:139–70.
48. Shinderman-Maman E, Cohen K, Weingarten C, Nabriski D, Twito O, Baraf L, et al. The thyroid hormone-alphavbeta3 integrin axis in ovarian cancer: regulation of gene transcription and MAPK-dependent proliferation. *Oncogene*. 2016;35:1977–87.
49. Cohen K, Ellis M, Khoury S, Davis PJ, Hercbergs A, Ashur-Fabian O. Thyroid hormone is a MAPK-dependent growth factor for human myeloma cells acting via alphavbeta3 integrin. *Mol Cancer Res*. 2011;9:1385–94.

ACKNOWLEDGEMENTS

The work of DM was done in partial fulfillment of the requirements for a PhD degree from the Sackler Faculty of Medicine, Tel Aviv University, Israel. OA-F and BL received

support from the Israel Innovation Authority, Nofar Program for Applied Research in Academia, Ministry of Economics (Project 59435).

AUTHOR CONTRIBUTIONS

DM preformed, analyzed, and interpreted the experimental data. AA, AR, and YF performed some of the methods. AW, AK, and DK assisted in the IHC assays. GM, TL, and BL designed and developed the DIO3 inhibitors. SM and HU performed enzymatic inhibition assays. OA-F designed, analyzed, and interpreted the experimental data. DM, GM, BL, ME, and OA-F wrote the manuscript. All authors read and approved the manuscript.

COMPETING INTERESTS

BL, GM, TL, and OA-F hold a patent for DIO3 inhibitors or are involved in patent commercialization. The other authors declare no potential conflict of interest.

ADDITIONAL INFORMATION

Supplementary information The online version contains supplementary material available at <https://doi.org/10.1038/s41388-021-02020-z>.

Correspondence and requests for materials should be addressed to Osnat Ashur-Fabian.

Reprints and permission information is available at <http://www.nature.com/reprints>

Publisher's note Springer Nature remains neutral with regard to jurisdictional claims in published maps and institutional affiliations.

Springer Nature or its licensor (e.g. a society or other partner) holds exclusive rights to this article under a publishing agreement with the author(s) or other rightsholder(s); author self-archiving of the accepted manuscript version of this article is solely governed by the terms of such publishing agreement and applicable law.